Prediction of Natural Guidewire Rotation Using an sEMG-based NARX Neural Network

Xiao-Hu Zhou[1,3], Gui-Bin Bian[1], Xiao-Liang Xie[1], Zeng-Guang Hou[1,2,3] and Jian-Long Hao[1,3]
[1]State Key Laboratory of Management and Control for Complex Systems,
Institute of Automation, Chinese Academy of Sciences, Beijing 100190, China
[2]CAS Center for Excellence in Brain Science and Intelligence Technology, Beijing 100190, China
[3]University of Chinese Academy of Sciences, Beijing 100049, China
Email: {zhouxiaohu2014, guibin.bian, xiaoliang.xie, zengguang.hou, haojianlong2012} @ia.ac.cn

***Abstract*—For the treatment of cardiovascular diseases, clinical success of percutaneous coronary intervention is highly dependent on natural technical skills and dexterous manipulation strategies of surgeons. However, the increasing used robotic surgical systems have been designed without considering manipulation techniques, especially surgical behaviors and motion patterns. This has driven research towards exploitation of natural manipulation skills in recent years. In this paper, natural guidewire manipulations are analyzed and predicted using an sEMG-based nonlinear autoregressive neural network with exogenous inputs. The relationship between natural endovascular manipulation and guidewire rotation is built through the network. Two experiments at different rotational speed were performed to verify the effectiveness and robustness of the applied model. The experimental results show that the average predictive root mean error of five subjects is 15.61° at the low speed and 21.85° at the high speed. These favorable results could be of interest to improve existing robotic surgical systems.**

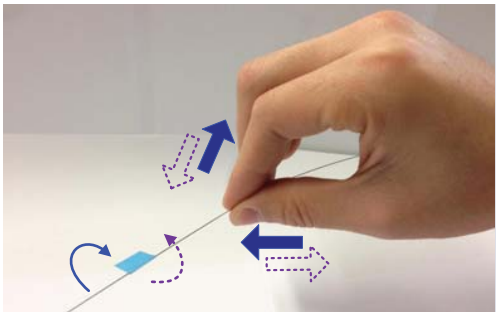

Fig. 1. Natural guidewire rotation. The surgeon moves the thumb and the forefinger in the opposite direction to rotate the guidewire: clockwise rotation (solid blue arrows) and counterclockwise rotation (dotted purple arrows).

I. Introduction

Cardiovascular diseases (CVDs) have become the biggest cause of death globally, and increasing people will be potentially plagued by CVDs [1]. Many companies and research institutions have developed some surgical robots to assist surgeons to manipulate interventional devices during endovascular intervention [2]. There is no doubt that these robotic systems can reduce the time that surgeons expose under X-ray radiation in operating theatre. However, most existing surgical robots have been designed without considering the ergonomic preferences and natural manipulation skills of experienced surgeons, such as finger and hand motion during endovascular procedures, which have been potentially altered through robotic solution [2]. Therefore, exploitation of natural manipulation skills during endovascular intervention is a matter of cardinal significance.

In the traditional procedures of percutaneous coronary intervention (PCI), the surgeon clamps a guidewire (or other interventional devices) with his thumb and forefinger and translates it along its axial direction by moving the whole hand at the same time. This translational manipulation makes the guidewire move along human vessel. The surgeon rotates the guidewire around its axis by moving the two fingers in the opposite direction that perpendicular to the guidewire's axis (see Fig. 1) [3]. There are numerous branches and bifurcations in human vascular system, thus rotational manipulation is essential to drive the guidewire to reach the right bifurcation. Finally, the guidewire is delivered to the blocked vessel or thrombus with the help of medical images guidance. In this delivery process, guidewire motion is often affected by its flexible body, small diameter (0.36 mm), variable blood flow and other uncertainties. These factors bring in time delay and motion error to its distal end, namely the rotational motion cannot be transferred along the guidewire effectively and accurately. Therefore, the motion of interventional devices is too complicated and unclear to model it easily.

In the past decades, some systems and methods in the field of surgery have been reported in the literature for studying surgeons' natural manipulation and analyzing the motion of surgical device. C. Tercero *et al.* [4] used optical sensors to encode a catheter's body motion, a magnetic tracker to capture the surgeon's hand motion, and opto-mechatronic sensors to measure the interaction between catheter tip and vasculature model wall, but manipulation flexibility is partly affected by these large number of sensors enclosed on the operator's hand. G. Srimathveeravalli *et al.* [5] analyzed human hand motion to identify design specifications for endovascular surgery and constructed a System for Endovascular Teleoperated Access (SETA) to simultaneously manipulate any guidewire and catheter in the range of 0.014-0.13 inches, but it is better to address the lack of natural twisting motions in the master to provide feedback. In [6], the surgeon's hand gestures in

978-1-5090-6182-2/17/$31.00 ©2017 IEEE

surgery was acquired with a wireless sensor glove to evaluate and assess surgical performance objectively, but the haptic sensing of hand and finger is lost more or less because of glove prevention. However, above analysis on predicting the motion of surgical devices, as well as building the relationship between the surgeon's natural manipulation and the motion of surgical devices are still limited.

Under the same motion state, the guidewire may be operated by experts and novices with different speed, force, rotational angle and translational distance [7]. According to medical images and feedback force from guidewire tip, experienced surgeons predict the guidewire motion and deliver the guidewire with more skilled technique and appropriate strategy than novices. There may be a signal that can give some assistance to surgeons for estimation and prediction of guidewire motion. Based on the above analysis, rotational angle of the guidewire is decided by the relative motion between the thumb and the forefinger [8]. According to the kinesiology of human body, finger motion is involved to regular contraction and relaxation of hand and arm muscles. These regular patterns are used to control finger motion during the delivery process, and different levels of surgeons have different motion patterns (experts' muscle motion patterns are different from novices'). Therefore, some features of hand and arm muscle can be considered as effective ways to evaluate surgeons' motion patterns and experience.

When skeletal muscles are in contraction, a micro-volt electrical activity named electromyogram is produced within muscle cells. This electrical signal can be measured non-invasively from skin surface and called *surface electromyography* (sEMG). With phase lead ahead of muscle stretch, sEMG is often used for decoding human motion pattern, joint angle or torque estimation, especially motion prediction in recent years [9]. In [10], an autoregressive model with first-order BP neural network was used to build the mapping relationship between multi-channel sEMG signals and joint angles. C. Loconsole *et al.* [11] used feedforward neural networks with augmented inputs (FNNAI) to predict the human shoulder and elbow joint torques with sEMG from relevant skeletal muscles. Some other researchers used nonlinear autoregressive neural networks (NAR) for small-scale solar radiation forecasting and energy consumption in public buildings prediction [12], [13].

Based on the above research, sEMG can be regarded as motion feature of natural guidewire rotation. An sEMG-based nonlinear autoregressive neural network with exogenous inputs (NARX) is applied to the prediction of natural guidewire rotation in this paper, which is a good embodiment of surgical skills and motion patterns that the surgeon estimates and predicts motion states of the guidewire in complex vascular environment. The performance of applied predictive method is evaluated and compared with NAR and FNNAI models. Experimental results demonstrate the applied NARX model has a good performance on rotation angle prediction. The remainder of this paper is organized as follows. Section II provides the sEMG-based NARX neural network and methods of data acquisition and processing. In Section III, the experimental design and results are given and discussed. Finally, the conclusion and future work are presented in Section IV.

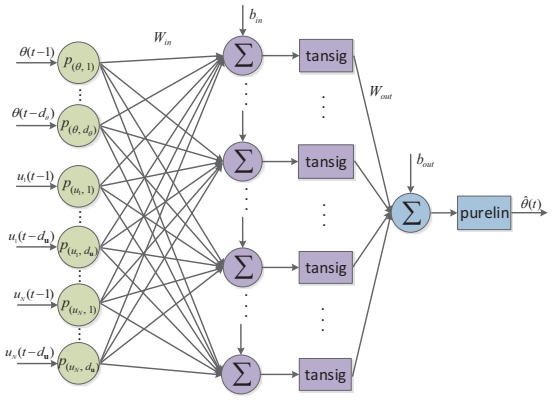

Fig. 2. The basic architecture of the NARX neural network.

II. Methods

A. sEMG-based NARX Neural Network

In this section, an sEMG-based model will be built to predict the rotation angle of the guidewire. The sEMG signals are the inputs of prediction model, while the output is the rotation angle of the guidewire. A NARX model is applied to expressing the relationship between the above two variables as follows:

$$\hat{\boldsymbol{\theta}}(t) = f(\boldsymbol{\theta}(t-1), \boldsymbol{\theta}(t-2), ..., \boldsymbol{\theta}(t-d_{\theta})... \\ \mathbf{u}(t-1), \mathbf{u}(t-2), ..., \mathbf{u}(t-d_{\mathbf{u}})) \quad (1)$$

where $\hat{\boldsymbol{\theta}}(t)$ is the predictive rotation angle at time t; $\boldsymbol{\theta}$ is the real measured one; $\mathbf{u}$ is a N-dimensional amplitude vector of multi-channel sEMG signals, namely $\mathbf{u}=\{u_1, u_2, ..., u_N\}$; N is the channel number of sEMG; d_{θ}, $d_{\mathbf{u}}$ are delay orders of feedback output and input; f is the functional expression between input and output [14]. Therefore Eq. (1) shows the relationship among current rotation angle, past angles and sEMG signals. The adopted model is based on linear ARX model, which is commonly used in time-series modeling [15]. In this paper, the applied model is implemented by using a feedforward neural network to approximate the function f. It is mainly composed of input layer, hidden layer, output layer and delay orders of input and output.

In this paper, the number of inputs is decided by the channel number of sEMG (N) and delay orders (d_{θ} and $d_{\mathbf{u}}$). We choose *tansig* as the transfer function of the hidden layer. The number of the hidden layer neurons n_h is adjusted according to network convergence, and its value is often estimated with empirical formulas. The transfer function of the output layer is *purline* and the rotation angle of the guidewire is the only network output. In order to reduce computation, the number of hidden layer is set as one and we select the number of neurons and delay orders as small as possible. The basic architecture

of the NARX neural network is shown in Fig. 2. The applied NARX neural network can be expressed as Eq. (2):

$$\hat{\theta}(t) = W_{out}[\frac{2}{1+e^{-2(W_{in}p+b_{in})}} - 1] + b_{out} \quad (2)$$

where W_{in} and b_{in} are the weight matrix and threshold vector of the hidden layer, W_{out} and b_{out} are the ones of the output layer. The input vector, p can be expressed as $p = [\theta(t-1), ..., \theta(t-d_\theta), \mathbf{u}(t-1), ..., \mathbf{u}(t-d_\mathbf{u})]$ in detail. The applied model can use the historical output data effectively because of feedback loop. In order to improve prediction accuracy, we use Bayesian regularization algorithm (*trainbr*) to train the NARX neural network. NAR (Eq. (3)) and FNNAI (Eq. (4)) models are adopted in this paper for comparison of predictive performance with NARX neural network [11], [12].

$$\hat{\theta}(t) = g(\theta(t-1), \theta(t-2), ..., \theta(t-d_\theta)) \quad (3)$$

$$\hat{\theta}(t) = h(\mathbf{u}(t-1), \mathbf{u}(t-2), ..., \mathbf{u}(t-d_\mathbf{u})) \quad (4)$$

B. Data Acquisition

A simulation system for guidewire manipulation is constructed to acquire rotation angle of the guidewire and sEMG signals from surgeons' skeletal muscles during endovascular procedures (Fig. 3). The system mainly consists of vascular model, electromagnetic (EM) tracking system (Aurora, Northern Digital Inc., Canada), sEMG acquisition device and PC. The vascular model is a linear acrylic tube installed on an acrylic table fixedly and the guidewire can be translated and rotated in it. The EM tracking system includes a 6-DOF EM sensor (Aurora, Northern Digital Inc., Canada) and magnetic field generator. The sensor is used to acquire rotation angle of the guidewire with the sampling rate 32 Hz. In order to measure the rotation angle of the guidewire accurately, the sensor and the guidewire are connected by a piece of guiding catheter for coaxial motion. The sEMG acquisition device researched by CASIA independently is used to collect sEMG signals from operators' relevant muscles. It can acquire sEMG signals with the frequency of 1024 Hz and eight channels acquisition at the same time. All acquisition programs run on a quad-core Intel Core i7-2600 PC. Before sEMG acquisition, some detail work, such as cleaning operators' skin and removing hair, is essential to reduce input resistance and external interference [9].

According to the analysis of natural guidewire rotation in Fig. 1, the relative motion between the thumb and the forefinger is applied to guidewire rotation and mainly involved in the abduction and adduction of the thumb and the flexion and extension of the forefinger, Thus a lot of muscles are involved in this complicated motion, mainly including *abductor pollicis brevis* (APB), *dorsal interossei* (DI), *flexor digitorum superficialis* (FDS) and *extensor digitorum* (ED). The sensitive muscles corresponding to guidewire rotation have been researched with principal components analysis (PCA) in our previous work [16]. In this paper, APB and DI are considered as sensitive and principal muscles during natural guidewire rotation.

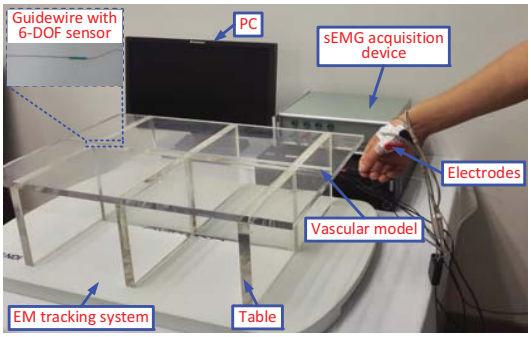

Fig. 3. The simulation system for guidewire manipulation. The guidewire can be manipulated in the acrylic vascular model and the sEMG signals from APB and DI is acquired simultaneously.

C. Data Processing

The limit frequency of sEMG signals is a range from 10 to 500 Hz and its main frequency band is 50-150 Hz. The sEMG is a very weak electrical signal due to its low amplitude (50 μV-30 mV). Therefore it is easily to be interfered by external noise in acquisition process. The external noise mainly comes from the following aspects: inherent noise, environmental noise, motion artifacts, baseline noise, industrial frequency interference (50 Hz in China). In this paper, the influence of DC noise is eliminated from the original sEMG signals with a differential amplifier firstly. Then the band-pass filter with frequency range of 20-500 Hz is used to remove motion artifacts and high frequency noise. In addition, industrial frequency interference is eliminated by a 50 Hz notch filter [10].

After filtering the noise, sEMG signals need to be further processed with the following steps:

1) Full-wave rectification: The amplitude of sEMG signals is random and vibrates near zero point frequently. Full-wave rectification can convert negative amplitude of sEMG signals to the positive half plane. It reflects amplitude characteristics of sEMG signals and can be expressed as:

$$u_{fwr}(n) = |u(n)| \quad (5)$$

where $u(n)$ is the nth original sEMG signal, $u_{fwr}(n)$ is the sEMG signal after full-wave rectification.

2) Normalization: Normalization is a non-dimensional method, which makes absolute values of variables become relative ones. In this paper, each channel of sEMG signals is normalized to maximal voluntary contraction (MVC).

$$u_{norm}(n) = \frac{u_{fwr}(n)}{|u_{MVC}|} \quad (6)$$

where u_{MVC} is the maximal voluntary contraction of sEMG signals, $u_{norm}(n)$ is the nth sEMG signal after normalization.

3) Sub-sampling: Because the sampling rate of the sEMG acquisition is 1024 Hz, which is much higher than the one of guidewire rotation measurement (32 Hz), sub-sampling is aim to keep the sampling rate of sEMG signals consistent with rotation angle of the guidewire. In addition, the calculation speed would be improved after sub-sampled. The process of sub-sampling can be expressed as:

$$u_{ss}(k) = \frac{1}{R} \sum_{i=(k-1)R+1}^{kR} u_{norm}(i) \tag{7}$$

where R is the ratio between sampling rates of sEMG signals and rotation angle, $u_{ss}(k)$ is the kth sEMG signal after sub-sampled.

4) Smoothing: In spite of the above processing steps, the envelope of sEMG signals is still severe. In fact, the amplitude of sEMG signals is only a measurement of muscle contraction and shows high frequency characteristics obviously, while the external performance of muscle contraction, namely rotation angle of the guidewire, shows low ones distinctly. Therefore a low-pass Butterworth filter (cut-off frequency is 5 Hz) is used to smooth sub-sampled signals in this paper.

III. Experiments and Results

Two experiments were designed to evaluate the performance of applied model in this section. In the first experiment, 5 subjects were recruited to rotate the guidewire at a low speed for 180° in clockwise direction firstly, and then for 180° in counterclockwise direction. Two manipulations are repeated for 65 seconds. Same to the first experiment, the guidewire are rotated at a high speed for only 45 seconds in the first experiment, because subjects' muscles would be fatigue after long time fast manipulation. Simultaneously, two-channel raw sEMG signals, as well as rotation angle of the guidewire are acquired and one trial data are shown in Fig. 4. For the slow rotation, the first 45 seconds of acquired data, are applied to training the NARX neural network, and the remaining 20 seconds data for testing the network, while the training and testing sets are the first 35 and the remaining 10 seconds respectively for the fast rotation. The root mean square error (*RMSE*) between the predictive rotation angle and real measured one in testing sets is calculated to evaluate the model performance. It can be expressed as:

$$RMSE = \sqrt{\frac{1}{M} \sum_{t=1}^{M} (\hat{\theta}(t) - \theta(t))^2} \tag{8}$$

where M is the number of sampling points.

A. Parameters Selection

For further simplicity, d_θ and d_u of the NARX neural network are set as the same in this paper (d=d_θ=d_u) [17]. After some attempts, we find that the predictive *RMSE* is no longer reduced when d is more than 10, because too much historical data could bring in redundant information, which leads to model oscillation. Furthermore, n_h has a greater impact on predictive performance than delay orders. Therefore, we set d as 2, 4, 6, 8, 10 and n_h as the even numbers between 1 and 20. Then the prediction of guidewire rotation with above combinations of d and n_h are performed and compared to select the optimal parameters. Fig. 5 and Fig. 6 present the average predictive performance of two speeds with different parameters. For the low speed, the curves of predictive *RMSE* become flat when n_h is more than 12. Less neuron in the hidden layer cannot describe the network exactly while more neurons could cause the network over fitting, increase model complication and time consumption. It is safely to know that the predictive performance of 4 delay orders is better than the others. Therefore, we choose the optimal parameters as 12 and 4 at the low rotational speed. For the high speed, the optimal parameters could be the same to the low speed according to Fig. 6 even if the predictive performance of 4 delay orders is slightly better than the performance of 2 delay orders, because a consistent network is better than two different ones for two different rotational speed. In addition, NAR and FNNAI models are all set as the same parameters to NARX neural network for performance comparison.

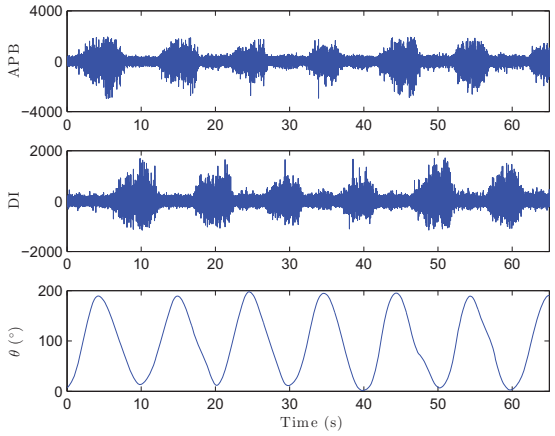

Fig. 4. Two-channel raw sEMG signals and rotation angle of the guidewire during a single trial from one of five subjects.

B. Prediction of Natural Guidewire Rotation

Three predictive models are trained and tested with the above optimal parameters. Fig. 7 presents the predictive performance of three models during one single trial at the low speed. In Fig. 7 (a), (b) and (c), the solid blue line is the actual measured rotation angles, and the dotted red, green and black lines are predictive angles of NARX, NAR and FNNAI models respectively. It is suggested that the predictive curve of the NARX neural network follows the actual measured angles more accurate than the other two models. Fig. 7 (d) shows the predictive error of NARX neural network is smaller than the others. Similarly, NARX neural network also shows better

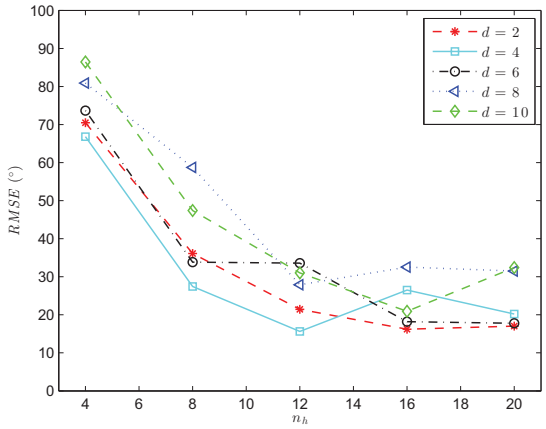

Fig. 5. The average *RMSE* of NARX neural network at the low rotational speed with different parameter combinations.

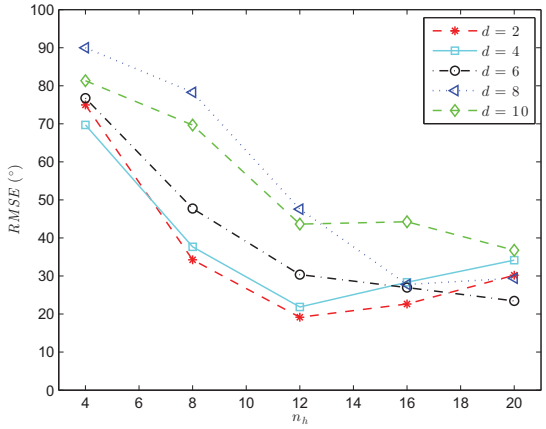

Fig. 6. The average *RMSE* of NARX neural network at the high rotational speed with different parameter combinations.

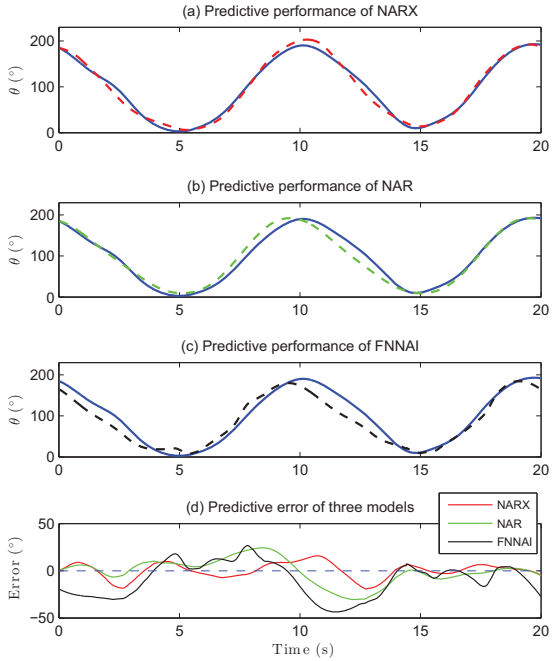

Fig. 7. Comparison of the actual rotation angles and the predictive ones at the low speed by using NARX, NAR and FNNAI models during a single trial from one of five subjects.

TABLE I
RMSE OF DIFFERENT MODELS AT THE LOW SPEED

Subject	*RMSE* (°)		
	NARX	NAR	FNNAI
S1	12.21	15.78	24.32
S2	15.46	20.06	25.95
S3	16.85	21.85	26.53
S4	17.91	23.43	27.18
S5	15.63	19.35	25.74
Mean	15.61	20.09	25.94

predictive performance than the other two models at the high speed in Fig. 8. This is because NARX model predicts rotation angle with both historical rotation angles and sEMG signals, while NAR model with only past rotation angles and FNNAI with only sEMG signals.

Table I and II show the *RMSE* of five subjects with three models. The average *RMSE* of each model is calculated and NARX neural network has the minimum one (15.61° at the low speed and 21.85° at the high speed). Such results are acceptable in practice because of small diameter of the guidewire. In addition, fast rotation shows larger *RMSE* obviously than slow rotation from two tables, since the EM tracking system has the poor performance of tracking fast rotation and some effective information may be lost during fast rotation process.

The predictive performance is also affected by the acquisition process of sEMG signals, because it is difficult to find the accurate positions of useful skeletal muscles and there is so much serious mutual interference among skeletal muscles. Furthermore, manipulation flexibility is affected more or less by the external wires of sEMG acquisition device.

IV. CONCLUSION AND FUTURE WORKS

This paper has proposed a new method for analyzing surgeons' natural motion patterns based on sEMG signals. A NARX neural network is adopted to predict the rotation angle of the guidewire during endovascular procedures and build the relationship between natural endovascular manipulation and guidewire rotation. The sEMG signals from APB and DI are considered as the exogenous inputs of the applied model and the recurrent dynamic output of the model is the rotation angles of the guidewire. The adopted model is implemented with a feedforward neural network and trained by the Bayesian regularization algorithm for improving the generation ability and predictive accuracy. Two experiments at the low and high speed are performed to evaluate the effectiveness and

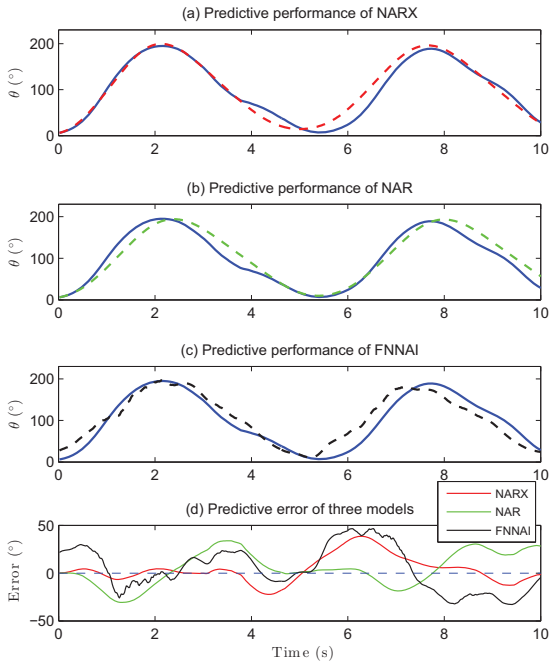

Fig. 8. Comparison of the actual rotation angles and the predictive ones at the high speed by using NARX, NAR and FNNAI models during a single trial from one of five subjects.

TABLE II
RMSE OF DIFFERENT MODELS AT THE HIGH SPEED

Subject	*RMSE* (°)		
	NARX	NAR	FNNAI
S1	18.35	22.05	26.98
S2	22.12	27.79	31.72
S3	23.85	28.03	32.56
S4	24.90	28.42	32.91
S5	20.05	23.87	30.34
Mean	21.85	26.03	30.90

robustness of the applied model. The experimental results reveal that the average predictive *RMSE* is 15.61° at the low speed and 21.85° at the high speed, which are more acceptable than NAR and FNNAI models. Therefore, NARX neural network supplies an effective method to predict natural guidewire rotation and evaluate surgical motion patterns and skills.

In future, NARX neural network will be used to further evaluate the distance of guidewire translation. The method of data mining and artificial intelligence will be applied to quantitatively analyzing surgical skills and experience. A surgical expert system using these acquired and processed skills will be constructed for autonomous or semiautonomous endovascular intervention in the future.

ACKNOWLEDGMENT

This research is supported by the National Natural Science Foundation (NNSF) of China (Grants 61533016, 61611130217, 61673379, U1613210 and 61421004), the Strategic Priority Research Program of the CAS (Grant XDB02080000), the Beijing science and technology project (Z161100001516004) and the Beijing Natural Science Foundation (Grant 4161001). The authors want to acknowledge the five student volunteers who participate in our experiments to obtain data samples.

REFERENCES

[1] S. Mendis, T. Armstrong, D. Bettcher, *et al*., "Global status report on noncommunicable diseases 2014," *World Health Organization*, Geneva, 2014.

[2] H. Rafii-Tari, C. J. Payne, and G.-Z. Yang, "Current and emerging robot-assisted endovascular catheterization technologies: a review," *Annals of Biomedical Engineering*, vol. 42, no. 4, pp. 697-715, 2014.

[3] Z. Q. Feng, G. B. Bian, X. L. Xie, Z. G. Hou, and J. L. Hao, "Design and evaluation of a bio-inspired robotic hand for percutaneous coronary intervention," in *Proceedings of 2015 IEEE International Conference on Robotics and Automation*, Seattle, USA, pp. 5338-5343, 2015.

[4] C. Tercero, H. Kodama, C. Shi, *et al*., "Technical skills measurement based on a cyber-physical system for endovascular surgery simulation," *The International Journal of Medical Robotics and Computer Assisted Surgery*, vol. 9, no. 3, pp. e25-e33, 2013.

[5] G. Srimathveeravalli, T. Kesavadas, X. Li, "Design and fabrication of a robotic mechanism for remote steering and positioning of interventional devices," *The International Journal of Medical Robotics and Computer Assisted Surgery*, vol. 6, no. 2, pp. 160-170, 2010.

[6] R. C. King, L. Atallah, B. P. Lo, and G.-Z. Yang, "Development of a wireless sensor glove for surgical skills assessment," *IEEE Transactions on Information Technology in Biomedicine*, vol. 13, no. 5, pp. 673-679, 2009.

[7] G. B. Bian, X. L. Xie, Z. Q. Feng, Z. G. Hou, *et al*., "An enhanced dual-finger robotic Hand for Catheter manipulating in vascular intervention: a preliminary study," in *Proceedings of 2013 IEEE International Conference on Information and Automation*, Yinchuan, China, pp. 356-361, 2013.

[8] X. H. Zhou, G. B. Bian, Z. G. Hou, *et al*., "Tracking Natural Guidewire Manipulations with an Improved Data Glove," in *Proceedings of IEEE International Conference on Robotics and Biomimetics*, Qingdao, China, pp. 1832-1837, 2016.

[9] F. Zhang, P. Li, Z. G. Hou, *et al*., "sEMG-based continuous estimation of joint angles of human legs by using BP neural network," in *Neurocomputing*, vol. 78, no. 1, pp. 139-148, 2012.

[10] L. Tong, F. Zhang, Z. G. Hou, *et al*., "BP-AR-Based human joint angle estimation using multi-channel sEMG," *International Journal of Robotics and Automation*, vol. 30, no. 3, 2015.

[11] C. Loconsole, S. Dettori, A. Frisoli, *et al*., "An EMG-based approach for on-line predicted torque control in robotic-assisted rehabilitation," in *Proceedings of 2014 IEEE Haptics Symposium (HAPTICS)*, Houston, USA, pp. 181-186, 2014.

[12] K. Benmouiza, A. Cheknane,, "Small-scale solar radiation forecasting using ARMA and nonlinear autoregressive neural network models," *Theoretical and Applied Climatology*, vol. 124, no. 3-4, pp. 945-958, 2016.

[13] L. G. B. Ruiz, M. P. Cullar, M. D. Calvo-Flores, *et al*., "An Application of Non-Linear Autoregressive Neural Networks to Predict Energy Consumption in Public Buildings," *Energies*, vol. 9, no. 9, pp. 684, 2016.

[14] E. Diaconescu, "The use of NARX neural networks to predict chaotic time series," *Wseas Transactions on computer research*, vol. 3, no. 3, pp. 182-191, 2008.

[15] T. Lin, B. G. Horne, P. Tino, C. L. Giles, "Learning long-term dependencies in narx recurrent neural networks," *IEEE Transactions on Neural Networks*, vol. 7, no. 6, pp. 1329-1338, 1996.

[16] X. H. Zhou, G. B. Bian, Z. G. Hou, *et al*., "PCA-Based muscle selection for interventional manipulation recognition," in *Proceedings of IEEE International Conference on Robotics and Biomimetics*, Qingdao, China, pp. 921-926, 2016.

[17] C. Cui, G. B. Bian, Z. G. Hou, *et al*., "sEMG-based prediction of human lower extremity movements by using a dynamic recurrent neural network," in *Proceedings of Control and Decision Conference (CCDC)*, Yinchuan, China, pp. 5021-5026, 2016.